

Effect of Wall Thickness and Build Quality on the Compressive Properties of 304L Thin-walled Structures Fabricated by SLM

Myranda Spratt¹, Sudharshan Anandan², Rafid M. Hussein², Joseph W. Newkirk^{1*},
K. Chandrashekhara², Heath Misak³, and Michael Walker³

¹Materials Science and Engineering Department

²Department of Mechanical and Aerospace Engineering

Missouri University of Science and Technology, Rolla MO 65409

³Spirit AeroSystems, Inc, Wichita, KS 67210

*Author for Correspondence (jnewkirk@mst.edu)

Keywords: Steel, SLM, Lattice

Abstract

The specific strength of lightweight lattice structures built with SLM is of interest to the aerospace industry. Honeycombs were manufactured with increasing wall thicknesses (which increases density) and tested under compression. The optimal strength to density ratio was determined from the resulting data. The build quality was also evaluated to determine how/if the results were influenced by the specimen quality. Differences between the nominal and as-built geometry were identified, but considered to be minimal. Microstructural evaluation of the specimens revealed a possible dependence on the ‘border scan’ properties, as the thickness of the specimens was such that the board scan made up most of the part. This work was used to validate the results of a finite element analysis of this geometry.

Introduction

Low density, high strength materials are used in a number of applications such as the aerospace [1] and automotive industries [2] and as lightweight protective equipment [3]. Carbon fiber reinforced polymers have been used recently in applications where weight saving is needed, such as in newer airplanes, but are limited by temperature. [4] Figure I is a material design chart [5] that shows the density-strength relationship of many composite and monolithic materials. As this chart shows, the specific strengths of most materials follow a linear trend on a log-log graph. Efforts to improve specific strength are on-going and often involve optimizing complex structures.

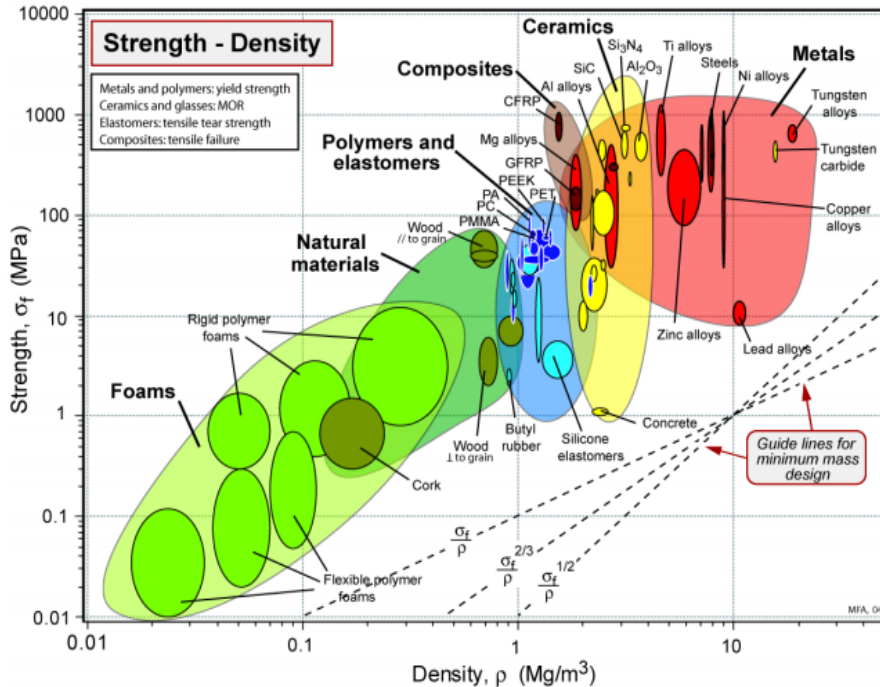


Figure I: Ashby material design chart for strength and density, where materials are plotted to show general trends. [5]

Lightweight structure design can be made simpler using finite element analysis (FEA) to create optimal structures, which can then be additively manufactured. Structures with complex geometries can be computationally intensive to optimize, so a unit cell approach can be used. A unit cell approach is typified by designing a unit cell which can be repeated in 2 or 3 dimensions to create the entire structure. A representative volume element (RVE) can then be selected to undergo FEA. Figure II shows three samples of unit cells – a 2D and 3D strut based design and a minimal surface design. The hexagonal honeycomb (the 2D strut based design) was selected for this experiment as it is the simplest of the three structures. Using mechanical property data for the material, a researcher can build a computationally-friendly RVE from the unit cell to represent the entire structure. This can then be optimized by FEA for the necessary application. In this process, all that is needed are the mechanical properties data for the SLM manufactured material and experimental validation of the results after FEA.

Digital models of components can be produced as a result of computational design. With only a few limitations, the digital model can then be fabricated with additive manufacturing. Additive manufacturing (AM) is a layer-by-layer process in which a digital component can be ‘sliced’ into layers and printed. There are several challenges to overcome when fabricating components with AM. One challenge is that the digital component, upon which any modeling is based, will not be perfectly reproduced with AM. Deviations from the model can include surface roughness, warpage due to residual stress, printing defects, and more. [6] AM-built components can also be anisotropic due to the layered material. [7] This runs contrary to most material

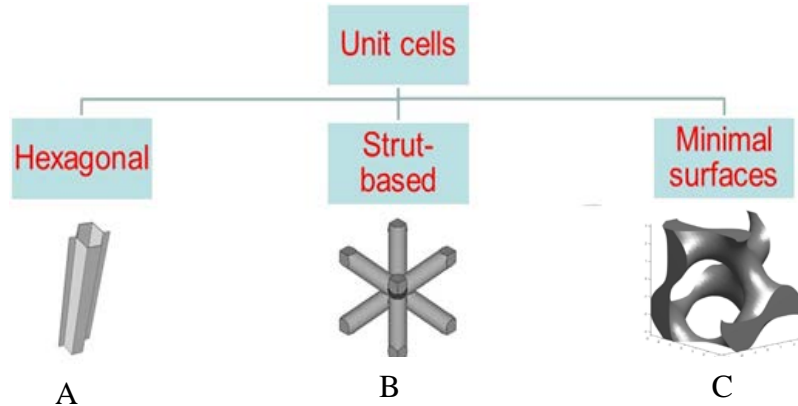


Figure II: Unit cell designs where A) is a 2D honeycomb, B) is a 3D body centered cubic strut design, and C) is a 3D gyroid minimal surface design.

models which assume the properties are isotropic. Other problems arise depending on the exact type of processing. Selective laser melting (SLM), for example, cannot print enclosed features without trapping powder within the component, which can be a major design limitation.

In this paper, the difference between the digital model of a honeycomb structure and the as-built component using simple physical measurements was determined. This difference can be used to inform the FEA model, the subject of a future paper. The compressive strength of honeycombs of increasing wall thickness was determined and compared to the strength to density of other materials. Finally, microstructure evaluation of the honeycombs after compression was used to aid in the failure analysis.

Materials and Methods

The honeycomb specimens were printed in a selective laser melting machine – a Renishaw AM250. 304L powder from LPW was used to build the specimens, in an argon atmosphere. The machine parameters were optimized for 304L and included a border scan optimized to decrease surface roughness and an internal scan optimized to increase density. The specimens were printed according to the specifications in Table I. They were removed from the build plate via wire electrical discharge machining (EDM), and cleaned with an ultrasonic bath to remove any remaining loose powder. Physical dimensions were measured with calipers. The density was determined using Archimedes’ method, with 95% isopropyl alcohol as the immersion liquid.

The specimens were compression tested using ASTM C365 at a strain rate of 3 mm/min. In each sample set, one specimen was randomly selected to not be tested. These specimens were sectioned, polished and etched to optically image the microstructure. After compression testing, other specimens were also selected for imaging. The specimens were electrolytically etched in a 60:40 nitric acid: water solution.

Table I: Sample dimensions as specified by the digital model.

| Sample Designations: | H1 | H2 | H3 | H4 |
|----------------------|-------|-------|-------|-------|
| Wall Thickness (mm) | 0.2 | 0.3 | 0.4 | 0.5 |
| Cell Size (mm) | 3.97 | 3.97 | 3.97 | 3.97 |
| Height (Z) | 25.4 | 25.4 | 25.4 | 25.4 |
| Width (W) | 25.15 | 25.73 | 24.38 | 20.83 |
| Length (L) | 26.67 | 27.28 | 26.67 | 22.86 |

Results and Discussion

Print accuracy was measured by comparing the CAD model of the honeycomb to the printed sample. Figure III shows a side-by-side view of the two. The dimensions measured were height, width, and length of the overall specimen, the cell size, and the wall thickness. Of all the measurements, only the wall thickness showed a statistically significant difference between the CAD model and the as-built samples. The details can be seen in Table II. The wall thickness was consistently larger than the CAD model, between 90 and 140 microns. This indicates that in the range of wall thicknesses tested, the accuracy of the Renishaw was generally good.

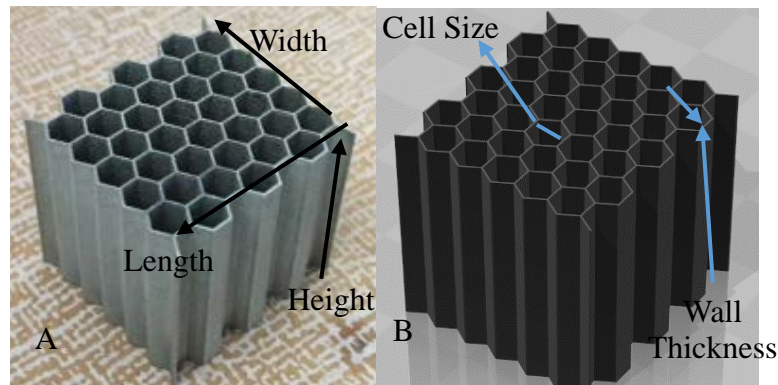


Figure III: Side-by-side view of the CAD model (A) and as-built (B) honeycombs.

Table II: Measured wall thickness compared to the digital model, with the standard deviation on each average value.

| Sample Designations: | H1 | H2 | H3 | H4 |
|------------------------------|----------|-----------|-----------|-----------|
| Nominal Wall Thickness (mm) | 0.2 | 0.3 | 0.4 | 0.5 |
| Measured Wall Thickness (mm) | 0.3±0.01 | 0.44±0.02 | 0.52±0.02 | 0.59±0.02 |

The difference between the nominal and measured wall thicknesses appears to be caused by a similar source across the samples. The deviation was attributed to the presence of powder particles sintered to the surface of the specimens. The size of the 304L powder was between 45 and 65 microns, which (when doubled to account for each wall of the specimens) corresponds to the increase in wall thickness from the CAD model to the as-built samples. These particles occur during the melting stage of the process. Particles can be heated due to proximity to the melt pool and can then weld to it. In a part where the surface area is very high (such as in these honeycomb samples), there is concern that these particles could detrimentally affect the mechanical properties of the component.

Investigation of the microstructure before and after compression testing reveals several key features about these structures. First, the surface particles sintered to the honeycomb walls are easily visible and correspond to the 45 to 65 micron range suggested above. Some of these particles are circled in Figure IV.A . Second, the melt pools and track boundaries are outlined in white after etching, with a dark feature within the bands. A close inspection of the dark features (Figure IV.B) finds that it is a cellular structure composed of dark and white features. Third, Figure V shows a honeycomb strut after compression testing. From this, and macro observation of the honeycomb, it was found that the honeycomb failed by local buckling near the center of the structure. Finally, there is very little porosity visible in these images, which indicates a high material density. This was confirmed by Archimedes density testing, which found that, on average, the density of the material was above 98% of theoretical.

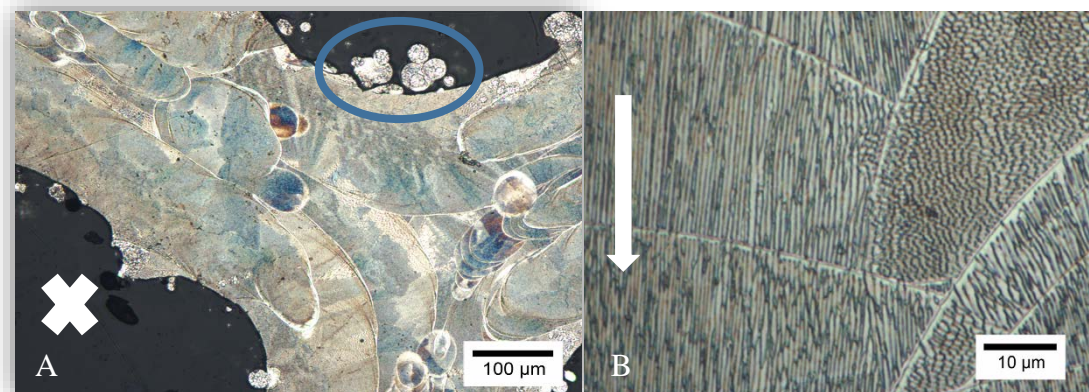


Figure IV: Honeycomb microstructures where A) shows a triple point and B) shows the cellular features. The blue circle shows particles welded to the walls, the white arrows show the build direction.

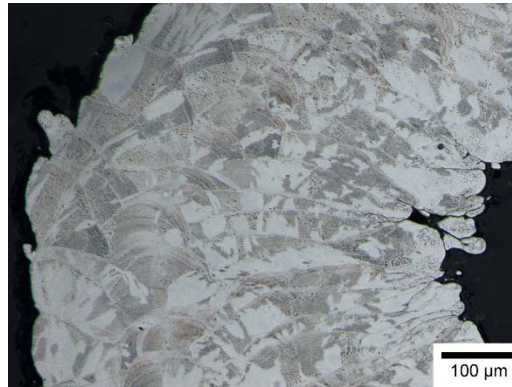


Figure V: A honeycomb strut that buckled after compression testing.

Table III shows the results of compression testing for each sample set. The density of the honeycombs increased from $\sim 1\text{g/cc}$ to $\sim 2\text{g/cc}$ as shown in Table III. The ultimate and yield strengths of the honeycombs increased as the density of the honeycombs increased, as expected. However, the specific yield stresses did not appear to increase as density increased, and though the specific ultimate strength did. The yield stresses of the honeycombs were plotted against the densities of the honeycombs on the material design chart in Figure VI [5]. The honeycombs yielded in the area marked as the polymers and elastomers region of the chart. They performed very similarly to most common plastics (PMMA, PEEK, PA, etc). The honeycombs could also be considered as an extension of the foam region as they follow a similar trend.

Table III: The results of compression testing the honeycomb samples, with the standard deviation on each average value.

| Sample Designations: | H1 | H2 | H3 | H4 |
|---|----------------|-----------------|-----------------|-----------------|
| Density ($\text{g/cm}^3 = \text{Mg/m}^3$) | 1.05 ± 0 | 1.46 ± 0.13 | 1.67 ± 0.02 | 1.97 ± 0.01 |
| Yield Stress (MPa) | 45.4 ± 2.2 | 54.8 ± 2.6 | 75 ± 3.8 | 83.3 ± 0.2 |
| Ultimate Stress (MPa) | 91.9 ± 9.1 | 132.8 ± 7.8 | 194 ± 2.4 | 267.1 ± 6.2 |
| Specific Yield (MPa/g/cm^3) | 43.2 ± 2.1 | 37.6 ± 1.8 | 44.9 ± 2.3 | 42.2 ± 0.1 |
| Specific Ultimate (MPa/g/cm^3) | 87.3 ± 8.5 | 81.8 ± 5.5 | 116.5 ± 2.1 | 134.4 ± 3.2 |

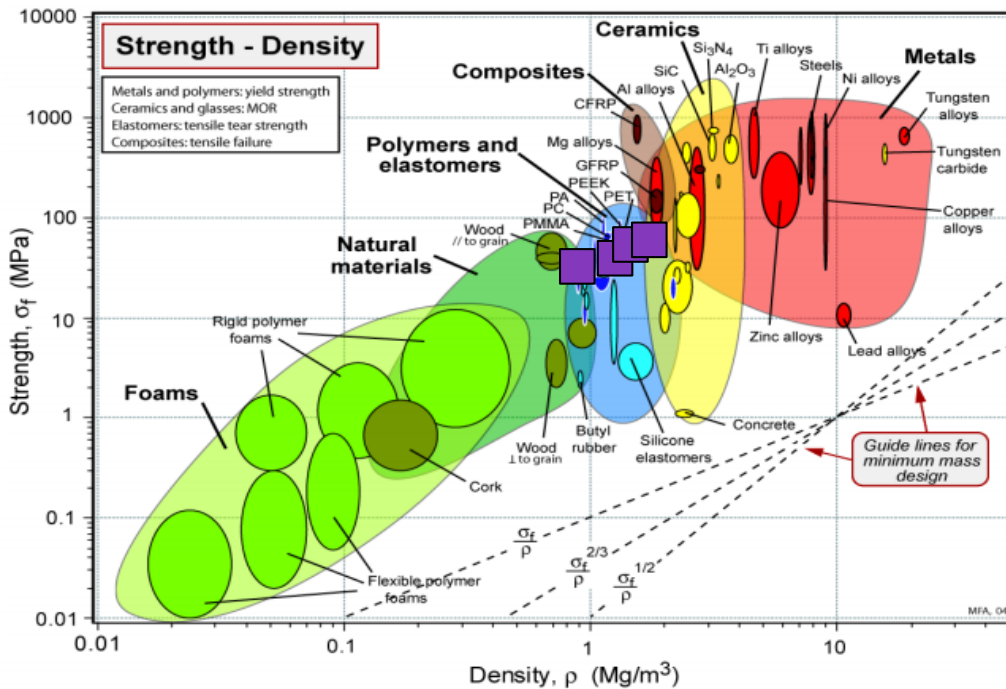


Figure VI: Strength-density chart including the yield stress data from this study (purple boxes). [5]

Conclusions

In conclusion, this study found that the honeycomb parts built with the Renishaw AM250 closely matched with the digital model. The only exception to this were particles that welded to the surface of the honeycombs during printing, which inflated the wall thickness of the honeycombs. Microstructural evaluation of the honeycombs found that localized buckling of the cell walls appears to have caused the honeycomb failure. The yield stress of the compressed samples, when graphed against other materials of the same density, was comparable to common structural plastics.

Acknowledgements

Support from Center for Aerospace Manufacturing Technologies (CAMT) at Missouri University of Science and Technology is gratefully acknowledged. The authors would also like to acknowledge Honeywell Federal Manufacturing and Technology for use of the Renishaw machine.

References

- [1] M. Standridge, Aerospace materials — past, present, and future, *Aerosp. Manuf. Des.* (2014). <http://www.aerospacemanufacturinganddesign.com/article/amd0814-materials-aerospace-manufacturing/> (accessed August 8, 2018).
- [2] T.P. Hovorun, K. V. Berladir, V.I. Pererva, S.G. Rudenko, A.I. Martynov, Modern materials for automotive industry, *J. Eng. Sci.* 4 (2017) f8–f18. doi:10.21272/jes.2017.4(2).f8.
- [3] Opportunities in Protection Materials Science and Technology for Future Army Applications, National Academies Press, Washington, D.C., 2011. doi:10.17226/13157.
- [4] F. Tanasa, M. Zanoaga, FIBER-REINFORCED POLYMER COMPOSITES AS STRUCTURAL MATERIALS FOR AERONAUTICS, n.d. <http://www.newairplane.com/787> (accessed August 8, 2018).
- [5] M.F. Ashby, CES 2009 Edupack: Material and Process Selection Charts, 1st ed., Granta Design Ltd, Cambridge, UK, 2009.
- [6] B. Song, X. Zhao, S. Li, C. Han, Q. Wei, S. Wen, J. Liu, Y. Shi, Differences in microstructure and properties between selective laser melting and traditional manufacturing for fabrication of metal parts: A review, *Front. Mech. Eng.* 10 (2015) 111–125. doi:10.1007/s11465-015-0341-2.
- [7] T. Niendorf, S. Leuders, A. Riemer, H.A. Richard, T.T. Ster, D. Schwarze, T. Tröster, D. Schwarze, Highly Anisotropic Steel Processed by Selective Laser Melting, *Metall. Mater. Trans. B.* 44 (2013) 794–796. doi:10.1007/s11663-013-9875-z.